Journal of Thermophysics and Heat Transfer
Vol. 37, No. 3, July–September 2023

Investigation on the Flow Instability of Supercritical Hydrocarbon Fuels in Cooling Channels

Yichao Jin,* Kun Wu,† Yang Lu,‡ and Xuejun Fan§
State Key Laboratory of High Temperature Gas Dynamics, Institute of Mechanics, Chinese Academy of Sciences, Beijing 100190, People's Republic of China

https://doi.org/10.2514/1.T6571

Flow instability in regenerative cooling channels is an important issue for the thermal protection of hypersonic scramjet engines. Taking into account the dynamic process of the heat transfer and flow instability, a one-dimensional transient model with several modules (including the cracking reaction, convective heat transfer, and rapid calculation of thermal properties) has been developed to investigate the flow instability characteristics of supercritical hydrocarbon fuels in cooling channels. The calculated results were compared and validated against the available experiments and numerical benchmarks, attaining good agreements. By virtue of the transient simulations, the dynamic flow patterns under different flow rates were studied in a single cooling channel with *n*-decane being the working substance. Then, the influences of the operating pressure and heated length on the in-tube flow were further investigated. In addition to the *Ledinegg* instability, several dynamic instability modes were detected under different external driving forces. It was also observed that under a specific range of pressure drop, the in-tube flow could transition from the density-wave oscillation to a new steady state. Moreover, this flow excursion was more likely to be triggered when decreasing the operating pressure or channel length.

Nomenclature

A	=	cross-sectional area, m^2
C_p	=	specific heat capacity, $J/(kg \cdot K)$
d	=	channel diameter, m
E	=	specific internal energy, J/kg
H	=	specific enthalpy, J/kg
h_{tc}	=	convection heat transfer coefficient, $W/(m^2 \cdot K)$
k	=	thermal conductivity, $W/(m \cdot K)$
k_F	=	chemical reaction rate, s^{-1}
L	=	length, m
m	=	mass flow rate, g/s
Nu	=	Nusselt number
N_{spc}	=	sub-pseudocritical number
N_{tpc}	=	trans-pseudocritical number
Pr	=	Prandtl number
p	=	pressure, Pa
$\dot{q}_w$	=	wall heat flux, W/m^2
$\dot{q}_c$	=	heat release or absorption due to cracking reaction, W/m^3
S	=	perimeter of the channel, m
T	=	temperature, K
t	=	time, s
u	=	velocity, m/s
V	=	volume, m^3
x	=	Cartesian coordinate in the x direction
Y	=	mass fraction
β_{pc}	=	thermal expansion number, K^{-1}
Δp	=	pressure drop in the heated channel, Pa
Δp_a	=	acceleration pressure drop, Pa
Δp_f	=	frictional pressure drop, Pa
Δp_t	=	external driving force, Pa
λ	=	friction coefficient
μ	=	viscosity, $Pa \cdot s$
ξ, η, ζ	=	coordinates in the three-dimensional table
ρ	=	density, kg/m^3

Subscripts

b	=	bulk
c	=	cracking reaction
F	=	fuel
f	=	fluid
q	=	inquiry point
w	=	solid wall

I. Introduction

FLOW instabilities induced by thermal load have been an important issue in the design and operation of industrial systems, such as steam generation [1], nuclear reactors [2,3], and electronic cooling systems [4]. Recently, the instability phenomena in regenerative cooling systems are also of great interest because of the worldwide development of scramjet engines [5]. During the cooling process, the hydrocarbon coolant may undergo phase change, which leads to heat transfer deterioration [6,7] and even flow instabilities [5,8]. Especially for the cooling systems constituting several parallel channels, locally germinated small perturbations could finally induce flow excursion under certain positive feedback, which severely affects the reliability of the cooling system.

Over the past decades, plenty of investigations into flow instability have been conducted, as pointed out by the review papers of Ruspini et al. [9] and Kakac and Bon [10]. The most common classification, introduced by Boure et al. [11], categories flow instabilities into static and dynamic instabilities. The static instability mainly behaves as the flow excursion among the equilibrium points. This phenomenon, also known as the Ledinegg instability, was first introduced by Ledinegg [12], which roots in the multivalued hydrodynamic characteristics of its internal characteristic curve, namely, the pressure drop versus mass-flow-rate characteristic curve. The unstable behavior can be predicted from the steady-state conservation laws. By comparing the slope at multiple intersection points between internal and external characteristic (supply pressure drop versus flow rate) curves, the one in the

Presented as Paper 2021-3719 at the AIAA Propulsion and Energy 2021 Forum, Virtual Event, August 9–11, 2021; received 19 January 2022; revision received 10 January 2023; accepted for publication 5 February 2023; published online 9 March 2023.

*Ph.D. Student, Institute of Mechanics; also School of Engineering Science, University of Chinese Academy of Sciences, 100049 Beijing, People's Republic of China; tdxh1993@buaa.edu.cn.
†Associate Professor, Institute of Mechanics; wukun@imech.ac.cn.
‡Associate Professor, Institute of Mechanics; luyang@imech.ac.cn.
§Professor, Institute of Mechanics; also School of Engineering Science, University of Chinese Academy of Sciences, 100049 Beijing, People's Republic of China; xfan@imech.ac.cn. Lifetime Member AIAA (Corresponding Author).

negative slope region of the internal characteristic curve is regarded to be unstable, and vice versa [13,14].

However, for dynamic instabilities, the periodic oscillations of the pressure, temperature, and mass flow rate are observed in the cooling channel. Hence, it is necessary to take into account the feedback effects of the flow rate and pressure drop to describe the behaviors of dynamic instabilities. Some frequency-domain methods [15–17] are usually used to obtain the stable boundary and describe the dynamic characteristics. Additionally, the compound instability is normally studied when the dynamic flow is acted upon by several basic mechanisms, e.g., the Ledinegg instability coupled with density-wave oscillation (DWO) [18] or pressure-drop oscillation [19]. In these complicated flows, linear and frequency-domain analyses become inadequate because strong nonlinearity is involved, and transient numerical calculation approaches are more attractive.

Recently, several one-dimensional models based on time-domain analysis have been reported in two-phase flows. Munoz-Cobo et al. [20] have established a reduced-order model to investigate the dynamic variations of pressure drop and inlet mass flux in parallel channels. Schlichting et al. [19] used a transient lumped parametrized model to investigate the dynamics of pressure-drop and density-wave oscillations. In the aforementioned models, the flow along the channel is simply divided into two sections based on the boiling boundary, which may be oversimplified for predicting the dynamics of hydrocarbon flow in the cooling channels. Meanwhile, more accurate one-dimensional methods were proposed in which more discrete subsections were incorporated to enhance prediction accuracy, e.g., the nonlinear homogeneous equilibrium model proposed by Clausse and Lahey [21]. Subsequently, Lee and Pan [22] and Guo et al. [23] further developed this model and expanded its application in two-phase flow instability of parallel multichannel systems, respectively. In addition to the homogeneous flow model, the drift-flux models that consider the relative velocity between the two phases have been widely reported, such as the works of Zanocco et al. [24] and Paul and Singh [25]. As for supercritical flow, Chen et al. [26], Lu et al. [27], and Ruspini et al. [28] have also developed more complex one-dimensional methods using various numerical discretization schemes.

It is obvious from the preceding brief review that the previous studies were mainly concerned with conventional fluids, such as water and carbon dioxide, whereas relevant work in supercritical hydrocarbon fuels is relatively rare. Besides, the physical properties of hydrocarbon fuels are very complicated due to their diverse components, resulting in notable uncertainty in modeling and expensive costs in the calculation. Significantly, the crack reactions [29,30] that arise under high temperatures will aggravate the challenge of analysis, which leads to a more complicated multivalued hydrodynamic problem. Therefore, it is essential to establish a one-dimensional transient calculation framework to attain an in-depth understanding of the instability behaviors of supercritical hydrocarbon flow in the cooling channels of regenerative cooling engines. In the present work, a one-dimensional transient calculation framework is proposed and validated for hydrodynamic instability in a single channel under supercritical operating conditions. Then, the dynamic characteristics are further investigated under various operating conditions and channel configurations.

II. Numerical Methodology

The theoretical formulation of the proposed numerical framework is briefly elaborated on in this section. The heated channel flow under supercritical conditions is quite complicated; thus, some assumptions and simplifications are required to achieve a feasible and reliable model. Referring to the previous research [21,22,26,27] on the two-phase and supercritical flow instabilities, a one-dimensional model is proposed to investigate the flow instabilities in the cooling channel with hydrocarbon fuels under supercritical conditions. To facilitate the physical modeling, the following assumptions are invoked in the current work:

1) The flow in the cooling channel is considered to be one-dimensional, and the flow variables are uniform on each cross section.
2) The heated channel is horizontal, and the gravity's effect is ignored.
3) The heat flux is uniformly distributed along the channel.
4) The viscous dissipation and mechanical work are neglected in the energy equation.
5) The cracking reaction is described using the proportional product distribution (PPD) model, and the diffusion effect is neglected.

Based on the preceding assumptions, the conservation equations for one-dimensional flow are summarized as follows:

$$\frac{\partial \rho}{\partial t} + \frac{\partial \rho u}{\partial x} = 0 \tag{1}$$

$$\frac{\partial \rho u}{\partial t} + \frac{\partial \rho u u}{\partial x} = -\frac{\partial p}{\partial x} - \frac{\lambda \rho u^2}{2d} \tag{2}$$

$$\frac{\partial \rho E}{\partial t} + \frac{\partial \rho u H}{\partial x} = \frac{\dot{q}_w S}{A} + \dot{q}_c \tag{3}$$

$$\frac{\partial \rho Y_F}{\partial t} + \frac{\partial \rho u Y_F}{\partial x} = -k_F \cdot \rho Y_F \tag{4}$$

where ρ is the density, u is the flow velocity, p is the pressure, E is the total internal energy, H is the total enthalpy, λ is the friction coefficient, S is the perimeter of the channel, and A is the cross-sectional area. Note that $\dot{q}_w$ is the surface heat flux, and $\dot{q}_c$ is the heat release or absorption due to cracking reactions.

A. Solution Procedure of Fluid Flow

To solve the aforementioned nonlinear partial differential equations, the semi-implicit scheme with the collocated grid is adopted to discretize the governing equations, as shown in Fig. 1. How each governing equation is discretized will be detailed in the following section.

Mass conservation equation:

$$\frac{\rho_i^{j+1} - \rho_i^j}{\Delta t} \Delta V_i + F_{f,i} - F_{f,i-1} = 0 \tag{5}$$

where ΔV_i is the cell volume, and $F_{f,i}$ is calculated as $F_{f,i} = 0.5\,(\rho_i u_i + \rho_{i+1} u_{i+1}) A$.

Momentum conservation equation:

$$\frac{\rho_i^{j+1} u_i^{j+1} - \rho_i^j u_i^j}{\Delta t} \Delta V_i + F_{f,i} \frac{u_i^{j+1} + u_{i+1}^{j+1}}{2} - F_{f,i-1} \frac{u_{i-1}^{j+1} + u_i^{j+1}}{2} = p_{f,i-1} A - p_{f,i} A - \frac{\lambda_i \rho_i^j u_i^j u_i^j \Delta L_i}{2d} A \tag{6}$$

Rearranging the preceding formula yields

$$A_{i,1} u_{i-1}^{j+1} + A_{i,2} u_i^{j+1} + A_{i,3} u_{i+1}^{j+1} = B_{i,u} + B_{i,p} \tag{7}$$

where

$$A_{i,1} = -\frac{F_{f,i-1}}{2} \quad A_{i,2} = \left(\frac{\rho_i^{j+1} \Delta V_i}{\Delta t} - \frac{F_{f,i-1}}{2} + \frac{F_{f,i}}{2} \right)$$

and

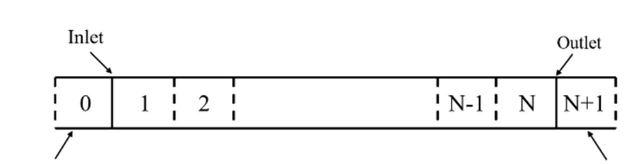

Fig. 1 Collocated grid for the semi-implicit scheme.

$$A_{i,3} = \frac{F_{f,i}}{2}$$

$B_{i,u}$ involves the explicit form of flow velocity because

$$B_{i,u} = \frac{\rho_i^j u_i^j \Delta V_i}{\Delta t} - \frac{\lambda_i \rho_i^j u_i^j u_i^j \Delta L_i}{2d} A$$

and $B_{i,p}$ denotes the source term induced by the pressure difference expressed as $B_{i,p} = (p_{f,i-1} - p_{f,i})A$. The friction coefficient λ is obtained by the Blasius correlation [31].

Energy conservation equation:

$$\frac{\rho_i^{j+1} E_i^{j+1} - \rho_i^j E_i^j}{\Delta t} \Delta V_i + F_{f,i} \frac{H_i^{j+1} + H_{i+1}^{j+1}}{2} - F_{f,i-1} \frac{H_{i-1}^{j+1} + H_i^{j+1}}{2} = \dot{q}_w S \Delta L_i + \dot{q}_c \Delta V_i \tag{8}$$

In the present work, the National Institute of Standards and Technology's NIST SUPERTRAPP software [32] is used to calculate the thermal properties of hydrocarbon fuels. To facilitate the formulation of the equation of state, the temperature and pressure are regarded as independent thermodynamic variables. Subsequently, the density and enthalpy can be linearized by the equation of state as

$$\rho_i^{j+1} - \rho_i^j = \left(\frac{\partial \rho}{\partial p}\right)_i^j \Delta p_i + \left(\frac{\partial \rho}{\partial T}\right)_i^j \Delta T_i \tag{9}$$

$$\rho_i^{j+1} E_i^{j+1} - \rho_i^j E_i^j = \left(H \frac{\partial \rho}{\partial p} + \rho \frac{\partial H}{\partial p} - 1\right)_i^j \Delta p_i + \left(H \frac{\partial \rho}{\partial T} + \rho \frac{\partial H}{\partial T}\right)_i^j \Delta T_i \tag{10}$$

After substituting Eqs. (9) and (10) into mass and energy equations, a combined matrix form can be obtained:

$$\begin{pmatrix} \Delta p \\ \Delta T \end{pmatrix}_i^j = \frac{\Delta t}{\Delta V_i} (\Phi_i^j)^{-1} \begin{pmatrix} DF1 \\ DF2 \end{pmatrix} \tag{11}$$

where

$$\Phi_i^j = \begin{pmatrix} \frac{\partial \rho}{\partial p} & \frac{\partial \rho}{\partial T} \\ H \frac{\partial \rho}{\partial p} + \rho \frac{\partial H}{\partial p} - 1 & H \frac{\partial \rho}{\partial T} + \rho \frac{\partial H}{T} \end{pmatrix}_i^j \tag{12}$$

$$DF1 = F_{f,i-1} - F_{f,i}$$
$$DF2 = F_{f,i-1} \frac{H_{i-1}^{j+1} + H_i^{j+1}}{2} - F_{f,i} \frac{H_i^{j+1} + H_{i+1}^{j+1}}{2} + \dot{q}_w S \Delta L_i + \dot{q}_c \Delta V_i \tag{13}$$

The preceding method is essentially a pressure-based algorithm, and the linear central scheme may lead to the checkerboard problem in the pressure field. Therefore, the Rhie–Chow interpolation scheme [33] is employed in this work to eliminate the pressure wave.

B. Cracking Model

Hydrocarbon fuel is a complex mixture with a large number of components, which leads to complex chemical mechanisms consisting of hundreds of species and reactions. However, to emphasize the characteristics of flow instability instead of the detailed chemical kinetic process, n-decane is considered as the surrogate fuel. For further simplification, the pyrolysis reaction is regarded as a first-order reaction in reference to Ref. [34]. The PPD assumption [35,36] is used to describe the pyrolysis reaction, and the overall reaction is specifically expressed as follows [35,36]:

$$\begin{aligned} C_{10}H_{22} \rightarrow\ & 0.153CH_4 + 0.222C_2H_4 + 0.138C_2H_6 + 0.200C_3H_6 \\ & + 0.185C_3H_8 + 0.171C_4H_8 + 0.118C_4H_{10} + 0.149C_5H_{10} \\ & + 0.137C_5H_{12} + 0.170C_6H_{12} + 0.106C_6H_{14} + 0.147C_7H_{14} \\ & + 0.091C_7H_{16} + 0.132C_8H_{16} + 0.040C_8H_{18} + 0.046C_9H_{18} \\ & + 0.031C_9H_{20} \end{aligned} \tag{14}$$

Thus, the conservation equation for the one-dimensional cracking reaction can be expressed as in Eq. (4). Y_F is the mass fraction of the reactant, and k_F is the chemical reaction rate obtained using the Arrhenius relation.

C. Calculation of the Thermal and Transport Properties

For complex hydrocarbon fuels, the calculations of thermodynamic and transport properties usually occupy more than 80% of the total CPU time; so, it is essential to reduce the cost of the thermal properties' calculation. To facilitate an efficient calculation, a lookup table method is applied in the present paper. First, the thermal and transport properties of the mixture are evaluated before the simulation and stored in a three-dimensional table (pressure p, temperature T, and mass fraction of reactant Y). Then, for each inquiry point (p_q, T_q, Y_q), the average value of the eight points in its nearest vicinity is used to improve numerical accuracy; and the calculation of the physical properties is outlined in Fig. 2. In the present work, the intervals of the pressure, temperature, and mass fraction are $\Delta p = 0.01$ MPa, $\Delta T = 2$ K, and $\Delta Y = 0.01$, respectively:

$$\xi = \frac{p - p_{\min}}{\Delta p}, \qquad \eta = \frac{T - T_{\min}}{\Delta T}, \qquad \zeta = \frac{Y - Y_{\min}}{\Delta Y} \tag{15}$$

D. Approach for Updating the Inlet Flow Rate

Affected by pressure feedback, the flow rate in the channel varies with time. In a previous study [37], the "Regula–Falsi" method was used to update the inlet flow rate. However, this method is wasteful in the multichannel parallel system due to extensive tentative calculations. Consequently, a more practical model has been proposed to solve the feedback relationship between the pressure and inlet flow rate. Referring to the model in Ref. [38], the cooling system is divided into two parts, namely, the entrance channel and the heated channel, as schematized in Fig. 3. The inlet pressure p_1 and the exit pressure p_3 are prescribed, whereas the inlet pressure of the heated section p_2 varies from time to time. Integrating over the entrance channel from zero to L_1, a lumped model can be obtained from the following momentum equation:

$$\frac{L_1}{A}\frac{dm}{dt} = p_1 - p_2 - \frac{\lambda \rho u^2 L_1}{2d} = p_1 - p_3 - (p_2 - p_3) - \frac{\lambda \rho u^2 L_1}{2d} = \Delta p_t - \Delta p - \frac{\lambda \rho u^2 L_1}{2d} \tag{16}$$

where Δp_t is the external driving force, and Δp is the pressure drop in the heated channel.

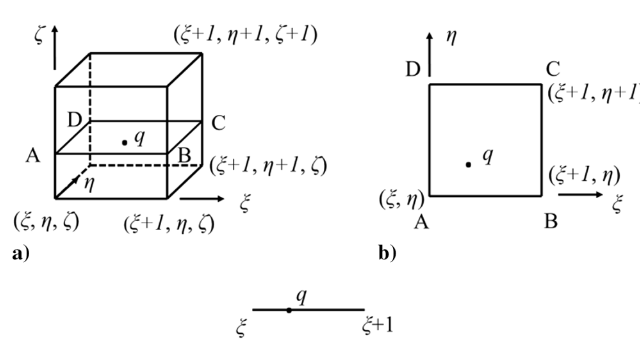

Fig. 2 Schematic diagrams of thermal and transport properties' calculations.

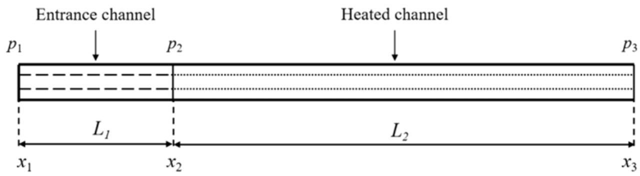

Fig. 3 Schematic diagram of the cooling channel along with the entrance channel.

In our implementation, the subsonic flow module is used to simulate the in-tube flow of the heated channel, and it provides Δp for the entrance channel. Then, the inlet flow rate is calculated in the entrance channel using Eq. (16) and supplied to the heated channel.

Based on the preceding numerical algorithms, an in-house code was developed to perform the calculation and then employed to investigate the flow instabilities of hydrocarbon fuel in cooling channels under supercritical conditions. To clarify the calculation process, the flowchart of the proposed calculation framework is summarized in Fig. 4.

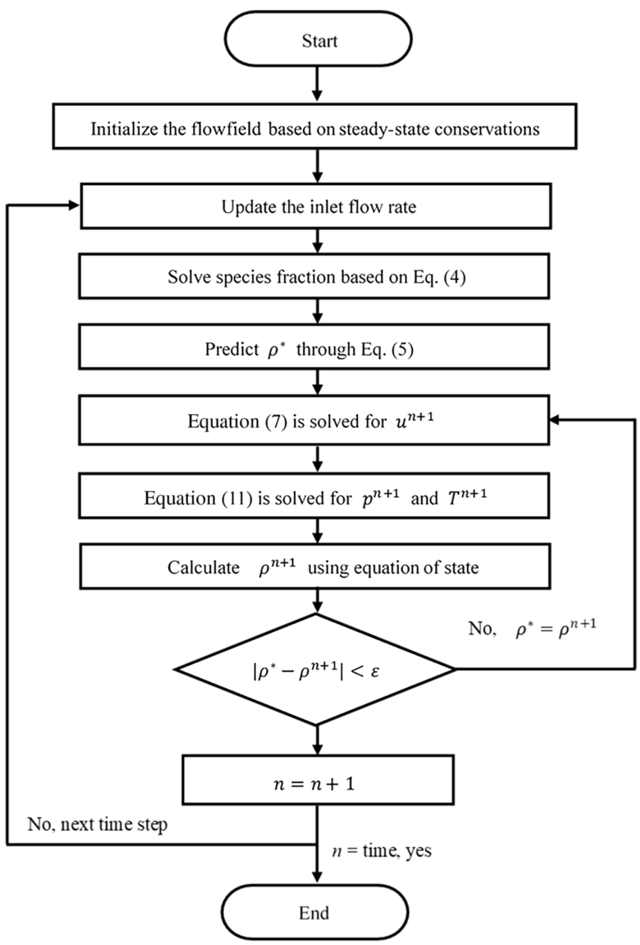

Fig. 4 Diagram of the numerical calculation procedure.

III. Model Validation

The heated channel flow using hydrocarbon fuels as coolant is extremely complicated, involving various physical issues such as the real-fluid effect, flow instability, heat transfer, and cracking reaction. To validate the reliability and accuracy of the new solver for those issues mentioned earlier in this paper, a series of test calculations has been conducted.

A. Lookup Table Method

Figure 5 compares the results obtained by direct calculation with SUPERTRAPP and the lookup table method under a cracking conversion rate of 32%. Compared to the direct calculation subroutine, a speedup ratio of around 50 has been achieved in the present work. It is also clear that excellent agreements between the two methods are obtained. The maximum relative error of the two methods is within 0.5%, which implies that the lookup table method gains acceptable accuracy.

B. Pressure Drop in the Channel

Referring to the experiments of Yang et al. [5], a circular tube with an internal diameter of 2 mm and a length of 670 mm is adopted as the benchmark. The corresponding critical parameters of the coolant are summarized in Table 1. As presented in Fig. 6, it shows that the calculated results agree well with the experimental measurements, except that the pressure drop is slightly underestimated in the small mass-flow-rate range. Overall, the positive and negative slope regions can be clearly distinguished in the calculation, and their mass-flow-rate ranges are reasonably compatible with the experimental observation. Thus, the capability of the present numerical framework in capturing the multivalued hydrodynamic characteristics (i.e., Ledinegg instability) is validated.

Table 1 Mass fractions and critical parameters of the fuels

	Mass fraction, %		Critical point	
Fuel	Pentane	Cyclohexane	Pressure, MPa	Temperature, K
Mix 1	100	0	3.37	469.75
Mix 2	30	70	3.60	491.60

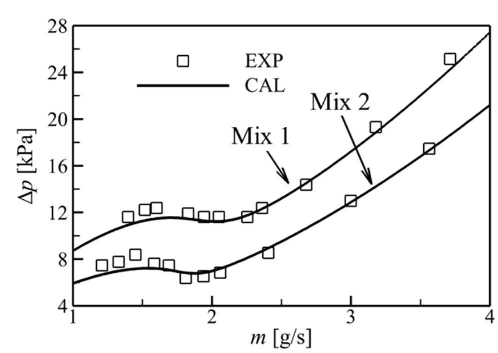

Fig. 6 Comparison between the present calculations (CAL) and the experimental data (EXP) at 4.5 MPa [5].

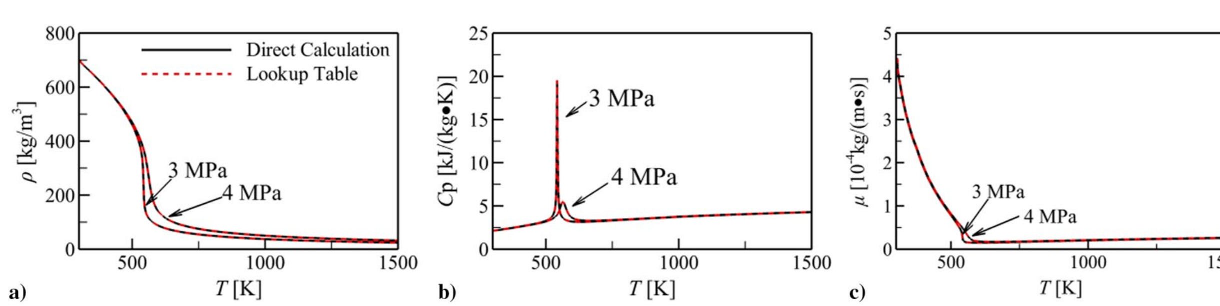

Fig. 5 Comparisons between the direct calculation and the lookup table method: a) density, b) heat capacity, and c) viscosity.

C. Cracking Reaction

In this section, the model validation was conducted by following the experiment of Ward et al. [35]. The tube is 0.5 mm in diameter and 375 mm in length, and the flow conditions of this experiment are listed in Table 2. The heat flux absorbed from the wall is calculated through the following formula:

$$q_w = h_{tc}(T_w - T_f) \tag{17}$$

where, $h_{tc} = Nu \cdot k/d$. N_u is the Nusselt number, which is obtained by the modified Dittus–Boelter correlation:

$$Nu = 0.023 Re_f^{0.8} Pr_f^{0.4} \left(\frac{\mu_f}{\mu_w}\right)^{0.11} \tag{18}$$

In Eq. (18), Re_f is the Reynolds number, Pr_f is the Prandtl number, μ_f is the viscosity coefficient at bulk temperature, and μ_w is the viscosity coefficient at the wall temperature. The transient model is concerned with fluid flows and heat transfer of n-decane with mild endothermic pyrolysis in a minitube. Variations of the conversion rate, bulk temperature, and fluid mixture density of n-decane are depicted in Fig. 7. The predicted results are quite consistent with experimental data under the operating conditions.

D. Unsteady Flow and Heat Transfer

To verify the simulation performance on the unsteady flow of the present model, the bulk temperature of methane in a heated channel is monitored. The test case follows the work in Ref. [39], in which the diameter of the heated tube is 2 mm and the length is 300 mm. Moreover, the inlet velocity is 25.0 m/s, the inlet temperature is 120 K, the exit pressure is 8.0 MPa, and the heated power ranges from 3 to 7 MW/m^2. Three different cases are simulated in this section, and the sampling point is in the middle of the heated channel. Despite its simplicity, the model agrees well with the simulation data by Ruan et al. [39], as shown in Fig. 8, which indicates that the proposed numerical framework can faithfully capture the dynamical response to the heating perturbation.

E. Stability Boundary for Density-Wave Oscillation

The proposed model is further validated against the benchmark of Ambrosini [40] to assess its capacity to predict dynamic instability. The operating conditions employed in the analysis are summarized in Table 3. The comparison of predicted results with existing data is shown in Fig. 9, where two dimensionless numbers are used to describe the stability boundaries, namely, the sub-pseudocritical number N_{spc} and the trans-pseudocritical number N_{tpc}:

Table 2 Operating conditions of the experiment

Parameter	Value
Flow rate, ml/min	0.5
Inlet temperature, K	423.15
Operating pressure, MPa	3.45
Maximum wall temperature, K	874

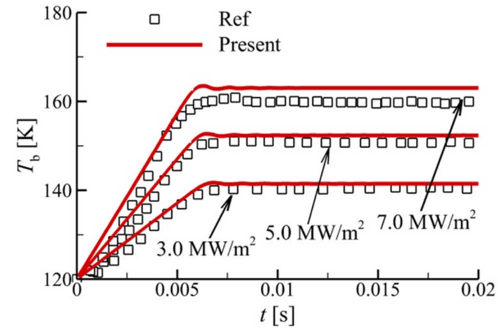

Fig. 8 Comparison between the numerical simulation and reference (Ref) data [39].

Table 3 Operating parameters for the heated channel under supercritical condition [40]

Property	Value
Pressure P, MPa	25
Critical pressure P_c, MPa	22.064
Pseudocritical temperature T_{pc}, K	373.95
Length L_H, m	4.2672
Diameter d_H, mm	8.36
Localized pressure-drop coefficient at inlet K_{in}	20
Localized pressure-drop coefficient at outlet K_{out}	20

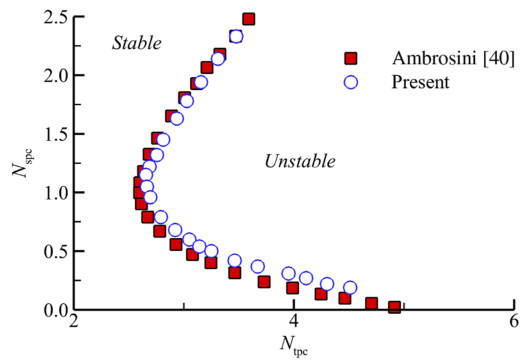

Fig. 9 Comparison of the stability boundary with data obtained in Ref. [40].

$$N_{spc} = \frac{\beta_{pc}}{C_{p,pc}}(h_{pc} - h_{in}); \quad N_{tpc} = \frac{q_w SL}{\rho_{in} u_{in} A} \frac{\beta_{pc}}{C_{p,pc}} \tag{19}$$

where β_{pc} is the thermal expansion number, $C_{p,pc}$ is the specific heat at constant pressure, and the subscript pc represents the pseudocritical state. As can be seen, the predicted results reasonably match the existing stability boundary [40], indicating that the model can be used to analyze the dynamic instability of supercritical fluid.

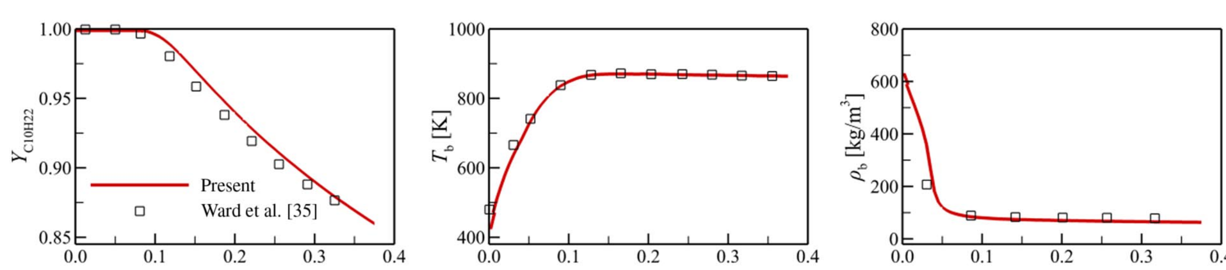

Fig. 7 Comparison between simulation and experiment data [35]: a) mass fraction of n-decane, b) bulk temperature, and c) density.

IV. Results and Discussion

By employing the present numerical framework, the flow dynamics in a single cooling channel are investigated under various operating conditions. Before the system response under the specific driving pressure drop can be evaluated, it is helpful to first determine the characteristics of its steady state. In Fig. 10, the pressure drop along a single horizontal pipe is presented as a function of the flow rate, for which the configurations and operating conditions are summarized in Table 4. These simulation settings are determined by referring to the heated minichannel experiments with supercritical hydrocarbon in Refs. [5,41].

Due to the drastic change of fluid density under supercritical conditions, there exists a negative slope region in the internal characteristic curve, which poses the multivalued phenomenon in heated channel flows. To facilitate the description of the stability patterns, the internal characteristic curve is divided into three parts, namely, the left branch, right branch, and negative slope region, as seen in Fig. 10a. As illustrated in Fig. 10b, there are three intersection points between the internal and external characteristic curves, with the operating point P being unstable. Correspondingly, a slight disturbance in the mass flow rate will lead to a spontaneous shift to the left equilibrium point P' or the right equilibrium point P''. This phenomenon involving a sudden change in the flow rate is the well-known Ledinegg instability.

A. Effect of the External Driving Force

Due to the flow hysteresis, the actual flow at the equilibrium point may not closely conform to the prediction obtained by the steady-state conservation laws. Therefore, the transient evolution of the in-tube flow deviating from the initial flowfield is conducted using the present model, and the effect of the external driving force is studied. The original state of the cooling channel is initialized using the steady flow of the mass flow rate of 2.5 g/s, which is approximately at the maximum in the internal characteristic curve. The external driving pressure drops are 12.0, 11.0, 10.8, 10.5, 10.4, 10.2, 10.1, and 10.0 kPa, respectively.

From the transient processes of the mass flow rate, as shown in Fig. 11, it is clear that the external driving pressure drop has a significant influence on the in-tube flow. On the equilibrium curve above the maximum point, there only exists one intersection point between two characteristic curves. Thus, the flow rate in the channel is attracted to this operating point, and it finally stabilizes at the right equilibrium point, as shown in Fig. 11a. The flow in the left branch is complicated and related to the external driving force. As the external driving force decreases, the trajectory of the mass flow rate transfers from a stable node to a limit cycle. To describe the channel flow in detail, the equilibrium curve for the steady-state solution is divided into four regions, namely, A, B, C, and D, as displayed in Fig. 10b. These were obtained from the simulations with various external driving forces.

1) In region A, the intrinsic mass flow rate and pressure drop are relatively lower than those of the maximum point. Subject to the lower driving force, the flow rate of the cooling channel decreases and then converges toward the left equilibrium point within a short time delay, as seen in Figs. 11b and 11c.

2) In region B, as compared to region A, the difference between the driving force and the initial pressure drop becomes larger and the dynamic instability appears in the channel; see the examples in Figs. 11d and 11e. The flow rate decreases first, and then flow oscillation starts after the flow excursion. The oscillation amplitude grows to a certain magnitude and then remains constant. Thus, the trajectory converges to a stable limit cycle. Besides, the oscillation's amplitude increases but the frequency decreases as the external driving force decreases.

3) In region C, the oscillation's amplitude of the flow rate increases significantly. If observing from the internal characteristic curve, the operating state can shift from the left branch to the right one. After being fully developed, the channel flow may stabilize at the right equilibrium point, such as in Fig. 11f.

4) In region D, the pressure drop is lower or slightly higher than the minimum of the internal characteristic curve. The transient flow rate can also cross the negative slope region and reach the right branch, but the right equilibrium point is very close to the minimum position or nonexistent. Under the action of the dynamic feedback of the system, it can no longer stabilize at the right branch of the characteristic curve. Hence, a low-frequency flow oscillation with a relatively large amplitude emerges, such as in Figs. 11g and 11h. Moreover, the oscillation's amplitude and frequency increase with the decrease of the external driving force.

Obviously, the results obtained by the transient model are not identical to those predicted by linear analysis based on the quasi-steady-state assumption. There exists an especially specific range in the internal characteristic curve, where the mass flow rate can oscillate from the left equilibrium point to the right one; and it finally stabilizes at the right branch. This phenomenon has yet to be reported in the previous literature.

To further illustrate the temporal evolution of the channel flow, a detailed discussion on several typical conditions is presented. Three operations with driving pressure drops of 10.4, 10.2, and 10.1 kPa are compared, as shown in Fig. 12. The limit cycle composed of inlet and outlet flow rates could be divided into three stages. The flow rates at the inlet and outlet decrease simultaneously, nevertheless the former to a more significant extent. Second, the inlet flow rate increases, whereas the outlet flow rate continues to reduce. Third, the outlet flow rate rises rapidly, whereas the flow rate at the inlet decreases slightly. In the third stage of flow evolution, the mass flow rate in the entire channel remains at the same level for a short period, which can be approximated as a steady state of the internal characteristic curve. If its pressure drop is less than the external driving force, the flow rate can overshoot to the right equilibrium point and stabilize at the right branch. On the other hand, in these large-amplitude oscillations, the

Table 4 Simulation conditions for the heated circular tube

Parameter	Value
Diameter, mm	2.0
Entrance length, mm	100
Heated length, mm	500
Inlet temperature, K	300
Inlet pressure, MPa	3.0
Heat flux, MW/m^2	1.0

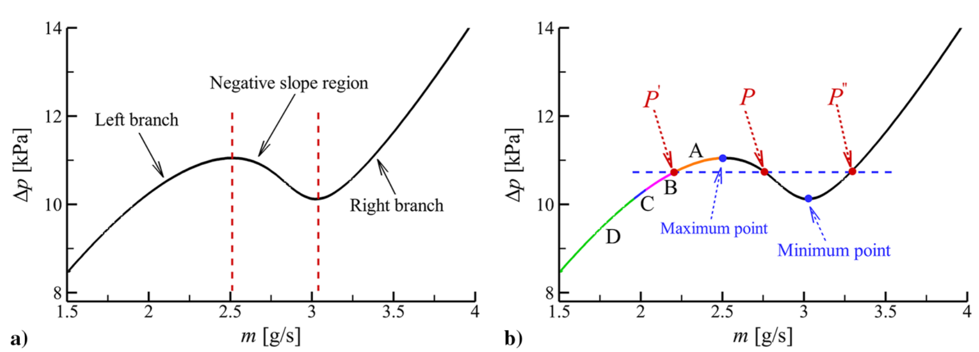

Fig. 10 Representations of a) internal characteristic curve, and b) intersection points between internal and external characteristic curves.

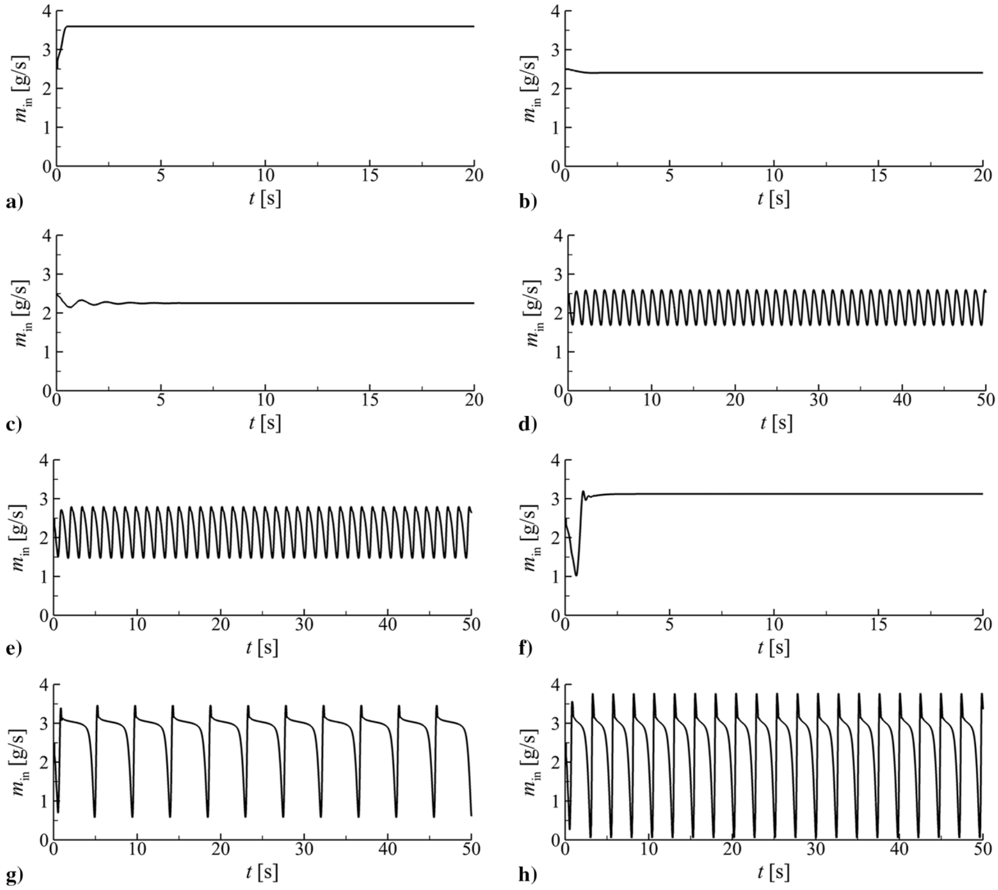

Fig. 11 Temporal evolutions of the mass flow rates under various driving pressure drops of a) 12.0, b) 11.0, c) 10.8, d) 10.5, e) 10.4, f) 10.2, g) 10.1, and h) 10.0 kPa.

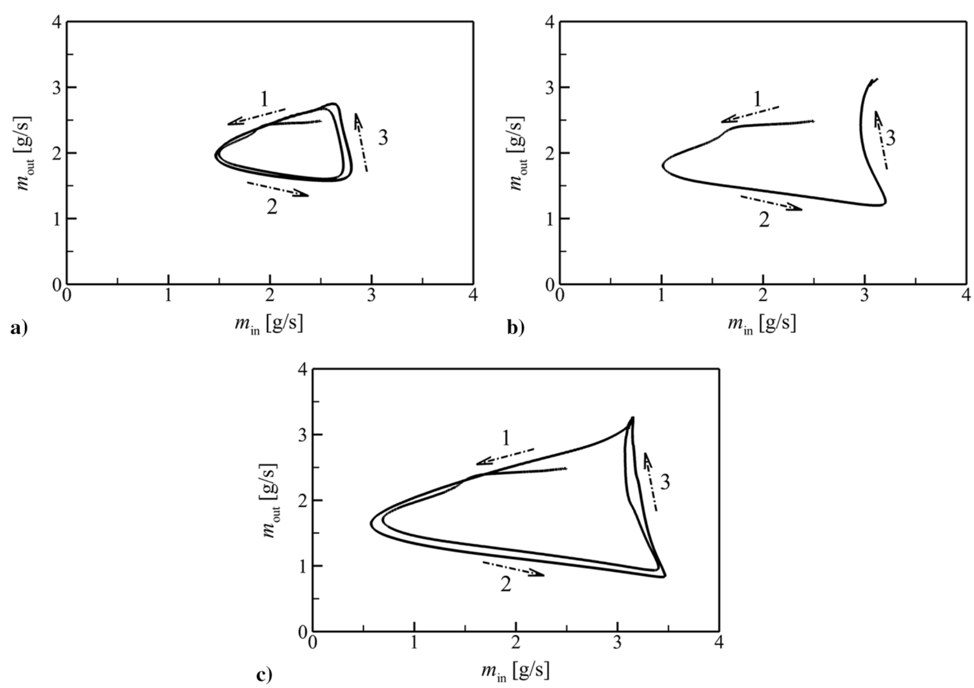

Fig. 12 Limit cycles under driving pressure drops of a) 10.4, b) 10.2, and c) 10.1 kPa.

negative slope region has a significant impact on in-tube flow evolution within the decreasing stage of the inlet mass flow rate. It narrows the gap between the external driving force and the pressure difference, leading to a period of slow flow rate changes. When the external driving force is especially close to the minimum value, the quasi-stable stage can be observed clearly in Fig. 11g.

B. Effect of Operating Pressure

Based on the previous research [10], the operating pressure has a crucial influence on fluid density, and even changes the flow stability. It is also worthwhile to discuss the stability behaviors of channel flow at various operating pressures. A series of pressure differences is calculated based on the steady state at the backpressures of 3.2 and

3.5 MPa. These internal characteristic curves are plotted in Fig. 13, and it is apparent that the operating pressure has remarkable influences on not only the negative slope region but also the left branch.

Two series of transient simulations are first conducted to intuitively exhibit the effect of operating pressure. These simulations are also

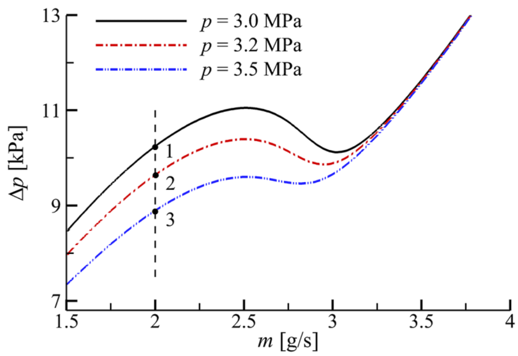

Fig. 13 Internal characteristic curves under various operating pressures.

Table 5 External driving forces for transient simulation

Group	External driving force, kPa		
	$\Delta p_{t,1}$	$\Delta p_{t,2}$	$\Delta p_{t,3}$
1	10.47	9.85	9.07
2	10.13	9.57	8.81

initialized using the steady flowfields with 2.5 g/s. The external driving forces (denoted as 1, 2, and 3 in Fig. 13) are selected based on the same flow rate. The conditions for the numerical study are summarized in Table 5, which are determined by referring to the internal curve at the flow rates of 2.05 and 1.95 g/s, respectively.

Figures 14 and 15 depict the two series of transient flows with different backpressures. In the former series, the channel flows behave as self-sustaining oscillations with a constant amplitude under an operating pressure of 3.0 MPa, whereas the trajectories of the flow rate converge to a stable node in the other two backpressures, as shown in Fig. 14. Reducing the mass flow rate, more flow patterns are detected in our simulations. As the operating pressure is increased from 3.0 to 3.5 MPa, the channel flow transforms from a low-frequency oscillation with large amplitude to a high-frequency self-sustaining oscillation, and then to the stable flow as shown in Fig. 15.

The oscillation types are now discussed in depth under different pressures, and they are summarized in Fig. 16. With the increase in backpressure, the flow rate maintains the same level at the maximum point while reducing visibly at the minimum point. As mentioned earlier in this paper, there are six main oscillation types for transient flow. When the backpressure is set to 3.0 MPa, the negative slope region starts at the flow rate of 2.51 g/s and ends at 3.02 g/s. The in-tube flow then becomes stable near the top of the left branch. As the mass flow rate continues to decrease to 2.21 g/s, DWO occurs behind the stable region. When the flow rate is reduced to 2.03 g/s, the operating state oscillates from the left equilibrium point to the right one. After the flow rate further decreases to 1.96 g/s, there is only an intersection point between external and internal characteristic curves. The low-frequency oscillation with large amplitude occurs in the following simulations.

With the pressure increasing to 3.2 MPa, the trajectory of the flow rate converges to the right equilibrium point when the mass flow rate

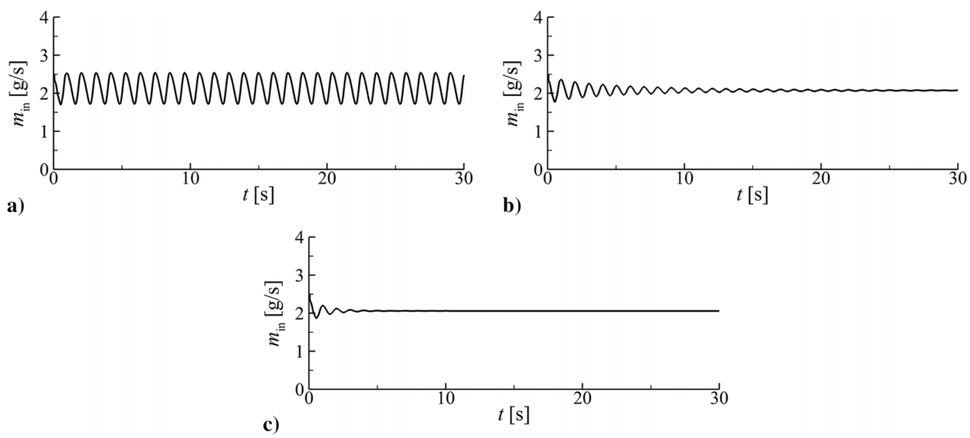

Fig. 14 In group 1, the temporal evolutions of the inlet flow rates under backpressures of a) 3.0, b) 3.2, and c) 3.5 MPa.

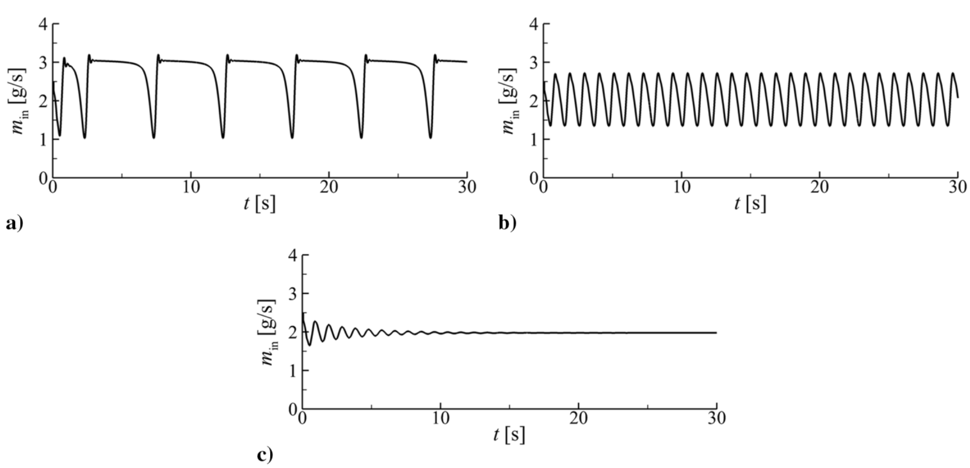

Fig. 15 In group 2, the temporal evolutions of the inlet flow rates under backpressures of a) 3.0, b) 3.2, and c) 3.5 MPa.

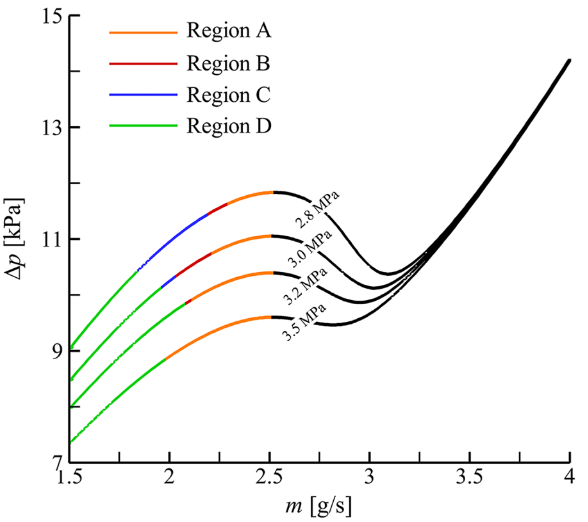

Fig. 16 Internal curves and flow instability types with various backpressures.

exceeds 2.95 g/s. The negative slope region is narrowed to the mass flow rate of 2.52–2.95 g/s, and the stable region in the left branch starts from 2.52 to 2.11 g/s. With the further decrease in the mass flow rate, DWO is also identified. When the flow rate is lower than 2.08 g/s, there only exists an operating point in the internal curve; so, the unstable flow in region C is not observed at this pressure. Immediately after region B, region D appears in the internal curve.

Under the pressure of 3.5 MPa, a substantial variation in fuel density owing to the phase transformation from liquid to gas could be avoided. The negative slope region is further narrowed, ranging from 2.52 to 2.82 g/s. The stable region is significantly broadened, and it is distributed from 1.98 to 2.52 g/s. And, the dynamic instability could be detected after the mass flow rate decreases to 1.98 g/s.

If the backpressure is decreased to 2.8 MPa, the negative slope region expands to range from 2.52 to 3.09 g/s. At this pressure, the flow instability is obviously enhanced. The stable region of the left branch distributes from 2.29 to 2.52 g/s, and DWO ranges from 2.19 to 2.29 g/s. Subsequently, the flow excursion from the left equilibrium point to the right one is measured at 1.84–2.19 g/s. This oscillation range expands dramatically as compared to the other test pressures. The low-frequency oscillation with a large amplitude is then detected in the lower part of the left branch.

To visually compare the effect of backpressure on flow instability, the oscillating amplitudes of the flow rate are illustrated in Fig. 17. The amplitudes are magnified greatly at low flow rates. For example, the amplitude in region D is significantly greater than in region B. It could also be concluded that dynamic flow would emerge at a lower flow rate if increasing the backpressures. Moreover, the trajectory of the flow rate tends to turn into the typical DWO because the negative slope region is shrank and the dynamic instability occurs away from the nadir. Thus, decreasing the backpressure would strengthen the flow instabilities, whether *Ledinegg* instability or the DWO instability.

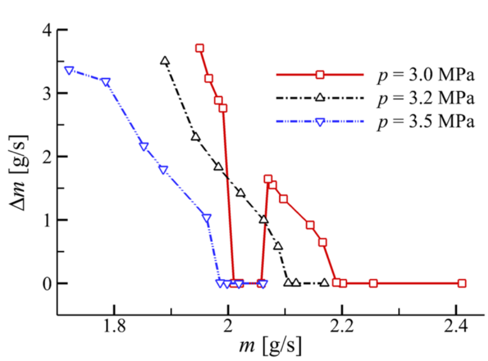

Fig. 17 Fluctuation amplitudes of inlet mass flow rate under different backpressures.

C. Effect of Channel Length

According to the previous study in Ref. [40], the nondimensional number N_{tpc} is a useful parameter to describe the stable boundaries in supercritical flow, which represents the heat absorbed by coolant. A similar fluid state could be detected in channel exit if adopting the same nondimensional number N_{tpc}. For dynamic flow, the flush through time is a key parameter in flow feedback. Thereby, the channel length may affect the evolution of channel flow. In this section, the effect of the heated length on dynamic characteristics is studied with a constant N_{tpc}.

The lengths of the heated channel are set to 400, 500, and 600 mm, with the same heating power of 3141.6 W. The other channel configurations, including channel diameter and entrance channel length, adopt the conditions in Table 4. Figure 18 depicts the internal curves, as well as the different types of dynamic flow. As the heated length increases, the pressure drop rises remarkably. Moreover, the negative slope region shrinks slightly, with the minimum point shifting to the left and the maximum point moving to the right. In the simulations with $L_2 = 400$ mm, the stable region is in the range of 2.24–2.48 g/s, and DWO occurs in the mass-flow-rate range of 2.13–2.24 g/s. The flow excursion from the left branch to the right one ranges from 1.85 to 2.13 g/s. The stable region is expanded to 2.18–2.55 g/s in these cases with $L_2 = 600$ mm, and DWO ranges from 2.06 to 2.18 g/s. Nevertheless, the flow excursion associated with region C is not detected, implying that the flow stability is enhanced.

To further investigate the effect of heated channel length, the total pressure drop is divided into three parts, as shown in Eq. (20):

$$\Delta p_{\mathrm{t}} = \Delta p_{f1} + \Delta p_{f2} + \Delta p_{\mathrm{a}} \tag{20}$$

in which Δp_{f1} is the frictional resistance of the entrance channel, Δp_{f2} is the frictional pressure drop of the heated channel, and Δp_{a} is the acceleration pressure drop. The components are depicted in Fig. 19, with data for the 500 mm case serving as a base reference. In Fig. 19b, L400_N and L600_N represent the channel length-based scaling results, which are calculated using Eq. (21):

$$\Delta p_{f2}^{*} = \Delta p_{f2} / \frac{L_{\mathrm{Ref}}}{L^{*}} \tag{21}$$

where L_{Ref} is 500 mm, and L^{*} denotes 400 and 500 mm, respectively. Obviously, only Δp_{f2} is affected distinctly by the heated channel in the present simulation, whereas the other two components are basically constant. These three coincident curves indicate that Δp_{f2} is

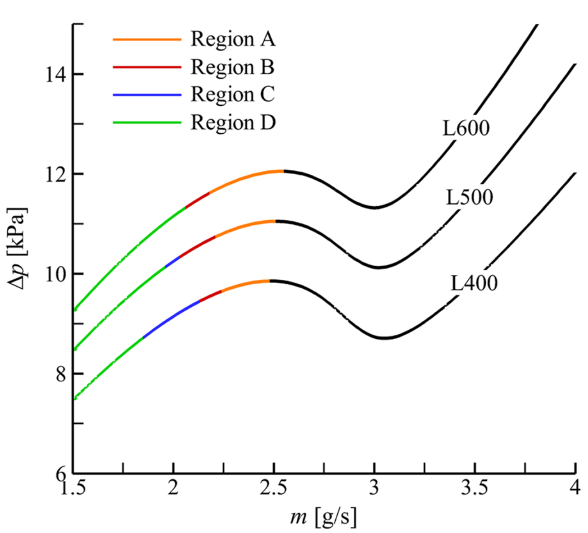

Fig. 18 Internal curves and flow instability types with various heated lengths.

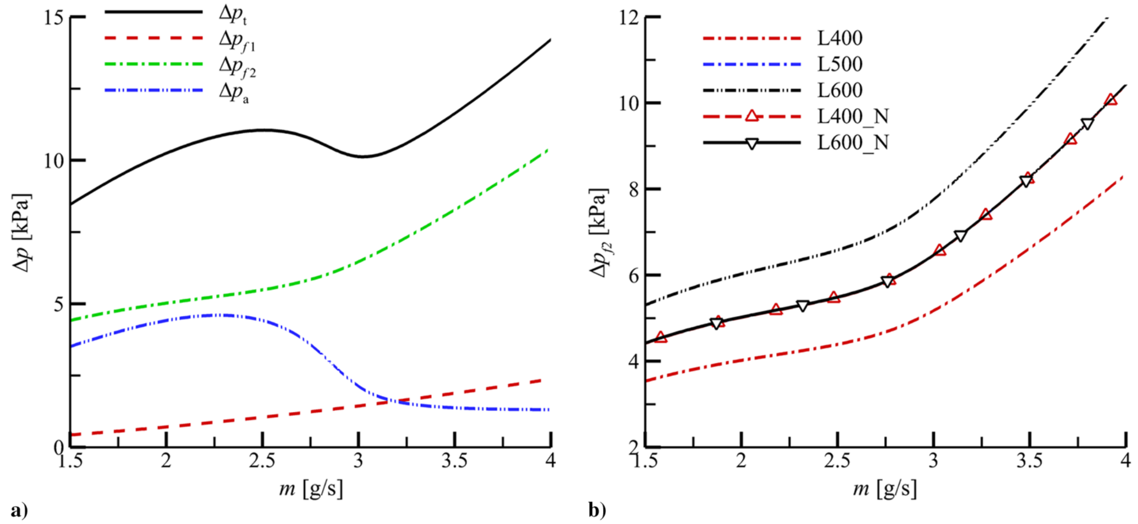

Fig. 19 Representations of a) pressure-drop components, and b) frictional pressure drops with various heated lengths.

proportional to the channel length. In Fig. 19a, it is clear that the acceleration pressure drop has a significant impact on flow instability, making a considerable contribution to the negative slope region. At high flow rates, the acceleration pressure drop accounts for a relatively small proportion of the total pressure drop; whereas at low flow rates, it is nearly equivalent to the frictional pressure drop. For DWO flow, the difference in flow momentum between the entrance and exit is also a significant source of dynamic feedback. The extension of the heated channel would reduce the contribution of the acceleration pressure drop to flow feedback. The increased flow through time and the flow inertia lead to a more stable flow, as observed in our simulations.

V. Conclusions

To deepen the understanding of the flow characteristics of supercritical hydrocarbon fuels in regenerative cooling systems, this paper developed a one-dimensional transient simulation model. The reliability of the model was assessed by comparing its results against the associated experiments and existing numerical simulations. Then, the effects of the external driving pressure drop, the operating pressure, and the heated length on the flow evolution were thoroughly discussed in the cooling channel using *n*-decane. The main conclusions are as follows:

1) The calculated results in this paper are in good agreement with the relevant experimental data and numerical simulations, which indicate that the present transient model is reliable to study the problem of flow instability in the cooling channels using hydrocarbon fuels. By exploiting this model, it is helpful to deepen the understanding of the mechanism of flow instability for flows under supercritical conditions in the cooling channels.

2) Through a series of transient simulations, it is observed that the operating point on the right branch is stable, whereas the one working in the negative slope region is unstable, which is consistent with the prediction by linear stability analysis. The in-tube flow is more complex on the left branch. As the external driving force decreases, it can be divided into several scenarios:

a) when the operating point is close to the maximum point, the flow in the cooling channel is stable.

b) The flow pattern transforms from a stable node into a limit cycle with a constant-oscillation amplitude. Besides, as the external pressure drop decreases, the amplitude increases but the frequency decreases.

c) The in-tube flow oscillates from the left equilibrium point to the right one, and it finally stabilizes at the right branch.

d) The channel flow behaves as a low-frequency oscillation with a relatively large amplitude. Moreover, both the oscillation's amplitude and frequency increase with a decreased external driving pressure drop.

3) Increasing the operating pressure would improve flow stability as follows:

a) The maximum flow rate that triggers dynamic instability decreases.

b) The range where the flow excursion oscillating from the left branch to right one shrinks and even disappears.

c) The negative slope region shrinks, weakening the influence on flow dynamics at low flow rates.

4) It also demonstrates that the acceleration pressure drop plays an important role in the dynamic flow because it contributes significantly to flow feedback in the cooling channels with a small length-to-diameter ratio. The pressure-drop curve becomes gentler in the negative slope region as the heated length increases, which is favorable for suppressing the flow instability.

Acknowledgments

This work was supported by National Key Project (grant no. GJXM92579). The authors are also grateful to National Supercomputer Center in Tianjin for providing the computational resources.

References

[1] Shin, C. W., and No, H. C., "Experimental Study for Pressure Drop and Flow Instability of Two-Phase Flow in the PCHE-Type Steam Generator for SMRs," *Nuclear Engineering and Design*, Vol. 318, July 2017, pp. 109–118.
https://doi.org/10.1016/j.nucengdes.2017.04.004

[2] Rohde, M., Marcel, C. P., T'Joen, C., Class, A. G., and van der Hagen, T. H. J. J., "Downscaling a Supercritical Water Loop for Experimental Studies on System Stability," *International Journal of Heat and Mass Transfer*, Vol. 54, Nos. 1–3, 2011, pp. 65–74.
https://doi.org/10.1016/j.ijheatmasstransfer.2010.09.063

[3] Paul, S., "On Nuclear-Coupled Thermal-Hydraulic Instability Analysis of Super-Critical-Light-Water-Cooled-Reactor (SCLWR)," *Progress in Nuclear Energy*, Vol. 117, Nov. 2019, Paper 103051.
https://doi.org/10.1016/j.pnucene.2019.103051

[4] Zhang, T. J., Wen, J. T., Peles, Y., Catano, J., Zhou, R., and Jensen, M. K., "Two-Phase Refrigerant Flow Instability Analysis and Active Control in Transient Electronics Cooling Systems," *International Journal of Multiphase Flow*, Vol. 37, No. 1, 2011, pp. 84–97.
https://doi.org/10.1016/j.ijmultiphaseflow.2010.07.003

[5] Yang, Z. Q., Li, T. H., Zhao, X., Gao, T. Z., and Zhang, B., "Hydrodynamic and Heat Transfer Characteristics of Binary Hydrocarbons at Trans- and Supercritical Pressures," *Experimental Thermal and Fluid Science*, Vol. 116, Aug 2020, Paper 110128.
https://doi.org/10.1016/j.expthermflusci.2020.110128

[6] Nasuti, F., and Pizzarelli, M., "Pseudo-Boiling and Heat Transfer Deterioration While Heating Supercritical Liquid Rocket Engine Propellants," *Journal of Supercritical Fluids*, Vol. 168, Feb. 2021, Paper 105066.
https://doi.org/10.1016/j.supflu.2020.105066

[7] Urbano, A., and Nasuti, F., "Onset of Heat Transfer Deterioration in Supercritical Methane Flow Channels," *Journal of Thermophysics and Heat Transfer*, Vol. 27, No. 2, 2013, pp. 298–308.
https://doi.org/10.2514/1.T4001

[8] Pan, H., Bi, Q., Liu, Z., Song, F., and Fan, F., "Experimental Investigation on Thermo-Acoustic Instability and Heat Transfer of Supercritical Endothermic Hydrocarbon Fuel in a Mini Tube," *Experimental Thermal and Fluid Science*, Vol. 97, Oct. 2018, pp. 109–118.
https://doi.org/10.1016/j.expthermflusci.2018.03.017

[9] Ruspini, L. C., Marcel, C. P., and Clausse, A., "Two-Phase Flow Instabilities: A Review," *International Journal of Heat and Mass Transfer*, Vol. 71, April 2014, pp. 521–548.
https://doi.org/10.1016/j.ijheatmasstransfer.2013.12.047

[10] Kakac, S., and Bon, B., "A Review of Two-Phase Flow Dynamic Instabilities in Tube Boiling Systems," *International Journal of Heat and Mass Transfer*, Vol. 51, Nos. 3–4, 2008, pp. 399–433.
https://doi.org/10.1016/j.ijheatmasstransfer.2007.09.026

[11] Boure, J., Bergles, A., and Tong, L., "Review of Two-Phase Flow Instability," *Nuclear Engineering and Design*, Vol. 25, No. 2, 1973, pp. 165–192.
https://doi.org/10.1016/0029-5493(73)90043-5

[12] Ledinegg, M., "Instability of Flow During Natural and Forced Circulation," *Die Waerme*, Vol. 61, No. 8, 1938, pp. 891–898.

[13] Padki, M. M., Palmer, K., Kaka, S., and Veziroglu, T. N., "Bifurcation Analysis of Pressure-Drop Oscillations and the Ledinegg Instability," *International Journal of Heat and Mass Transfer*, Vol. 35, No. 2, 1992, pp. 525–532.
https://doi.org/10.1016/0017-9310(92)90287-3

[14] Ghione, A., Noel, B., Vinai, P., and Demaziere, C., "Criteria for Onset of Flow Instability in Heated Vertical Narrow Rectangular Channels at Low Pressure: An Assessment Study," *International Journal of Heat and Mass Transfer*, Vol. 105, Feb. 2017, pp. 464–478.
https://doi.org/10.1016/j.ijheatmasstransfer.2016.10.012

[15] Zhang, Y., Li, H., Li, L., Wang, T., Zhang, Q., and Lei, X., "A New Model for Studying the Density Wave Instabilities of Supercritical Water Flows in Tubes," *Applied Thermal Engineering*, Vol. 75, Jan. 2015, pp. 397–409.
https://doi.org/10.1016/j.applthermaleng.2014.09.029

[16] Hou, S., Tai, Y., and Zhao, F., "Analysis of Instability for OTSG by Using Multivariable Frequency Domain Method," *17th International Conference on Nuclear Engineering*, ICONE17-75024, ASME, New York, 2009.
https://doi.org/10.1115/ICONE17-75024

[17] Guido, G., Converti, J., and Clausse, A., "Density-Wave Oscillations in Parallel Channels-An Analytical Approach," *Nuclear Engineering and Design*, Vol. 125, No. 2, 1991, pp. 121–136.
https://doi.org/10.1016/0029-5493(91)90072-P

[18] Singh, M. P., and Singh, S., "Non-Linear Stability Analysis of Supercritical Carbon Dioxide Flow in Inclined Heated Channel," *Progress in Nuclear Energy*, Vol. 117, Nov. 2019, Paper 103048.
https://doi.org/10.1016/j.pnucene.2019.103048

[19] Schlichting, W. R., Laheyjr, R. T., and Podowski, M. Z., "An Analysis of Interacting Instability Modes, in a Phase Change System," *Nuclear Engineering and Design*, Vol. 240, No. 10, 2010, pp. 3178–3201.
https://doi.org/10.1016/j.nucengdes.2010.05.057

[20] Munoz-Cobo, J. L., Podowski, M. Z., and Chiva, S., "Parallel Channel Instabilities in Boiling Water Reactor Systems: Boundary Conditions for Out of Phase Oscillations," *Annals of Nuclear Energy*, Vol. 29, No. 16, 2002, pp. 1891–1917.
https://doi.org/10.1016/S0306-4549(02)00024-5

[21] Clausse, A., and Lahey, R. T., "An Investigation of Periodic and Strange Attractors in Boiling Flows Using Chaos Theory," *Proceedings of the 9th International Heat Transfer Conference*, Jerusalem, Vol. 2, 1990, pp. 3–8.

[22] Lee, J. D., and Pan, C., "Dynamics of Multiple Parallel Boiling Channel Systems with Forced Flows," *Nuclear Engineering and Design*, Vol. 192, No. 1, 1999, pp. 31–44.
https://doi.org/10.1016/S0029-5493(99)00085-0

[23] Guo, Y., Qiu, S. Z., Su, G. H., and Jia, D. N., "The Influence of Ocean Conditions on Two-Phase Flow Instability in a Parallel Multi-Channel System," *Annals of Nuclear Energy*, Vol. 35, No. 9, 2008, pp. 1598–1605.
https://doi.org/10.1016/j.anucene.2008.03.003

[24] Zanocco, P., Gimenez, M., and Delmastro, D., "Modeling Aspects in Linear Stability Analysis of a Self-Pressurized, Natural Circulation Integral Reactor," *Nuclear Engineering and Design*, Vol. 231, No. 3, 2004, pp. 283–302.
https://doi.org/10.1016/j.nucengdes.2004.03.006

[25] Paul, S., and Singh, S., "A Density Variant Drift Flux Model for Density Wave Oscillations," *International Journal of Heat and Mass Transfer*, Vol. 69, No. 1, 2014, pp. 151–163.
https://doi.org/10.1016/j.ijheatmasstransfer.2013.10.012

[26] Chen, J., Gu, H., and Xiong, Z., "Development of One-Dimensional Transient Model for Predicting Flow Instability at Supercritical Pressures," *Progress in Nuclear Energy*, Vol. 112, April 2019, pp. 162–170.
https://doi.org/10.1016/j.pnucene.2018.12.014

[27] Lu, X., Wu, Y., Zhou, L., Tian, W., Su, G., Qiu, S., and Hong, Z., "Theoretical Investigations on Two-Phase Flow Instability in Parallel Channels Under Axial Non-Uniform Heating," *Annals of Nuclear Energy*, Vol. 63, Jan 2014, pp. 75–82.
https://doi.org/10.1016/j.anucene.2013.07.030

[28] Ruspini, L. C., Dorao, C. A., and Fernandino, M., "Dynamic Simulation of Ledinegg Instability," *Journal of Natural Gas Science and Engineering*, Vol. 2, No. 5, 2010, pp. 211–216.
https://doi.org/10.1016/j.jngse.2010.08.003

[29] Zhong, F., Fan, X., Yu, G., Li, J., and Sung, C., "Thermal Cracking and Heat Sink Capacity of Aviation Kerosene Under Supercritical Conditions," *Journal of Thermophysics and Heat Transfer*, Vol. 25, No. 3, 2011, pp. 450–456.
https://doi.org/10.2514/1.51399

[30] Gao, M., Guo, J., Pei, X., and Hou, L., "Aspect Ratio Effects on the Noncracking and Cracking Heat Transfer in Microchannels," *Journal of Thermophysics and Heat Transfer*, Vol. 36, No. 1, 2022, pp. 51–60.
https://doi.org/10.2514/1.T6252

[31] Incropera, F., DeWitt, D., Bergman, T., and Lavine, A., *Fundamentals of Heat and Mass Transfer*, 6th ed., Wiley, New York, 2006, pp. 486–497.

[32] Huber, M. L., *NIST Thermophysical Properties of Hydrocarbon Mixtures Database (SUPERTRAPP), Version 3.2: Users' Guide*, National Inst. of Standards and Technology, Gaithersburg, MD, 2007.

[33] Zhang, S., Zhao, X., and Bayyuk, S., "Generalized Formulations for the Rhie–Chow Interpolation," *Journal of Computational Physics*, Vol. 258, No. 1, 2014, pp. 880–914.
https://doi.org/10.1016/j.jcp.2013.11.006

[34] Qin, J., Jiang, Y. G., Feng, Y., Li, X. J., Li, H. W., Xu, Y. X., Bao, W., Zhang, S. L., and Han, J. C., "Flow Rate Distribute of Cracked Hydrocarbon Fuel in Parallel Pipes," *Fuel*, Vol. 161, Dec. 2015, pp. 105–112.
https://doi.org/10.1016/j.fuel.2015.08.015

[35] Ward, T. A., Ervin, J. S., Striebich, R. C., and Zabarnick, S., "Simulations of Flowing Mildly-Cracked Normal Alkanes Incorporating Proportional Product Distributions," *Journal of Propulsion and Power*, Vol. 20, No. 3, 2004, pp. 394–402.
https://doi.org/10.2514/1.10380

[36] Ward, T. A., Ervin, J. S., Zabarnick, S., and Shafer, L., "Pressure Effects on Flowing Mildly-Cracked n-Decane," *Journal of Propulsion and Power*, Vol. 21, No. 2, 2005, pp. 344–355.
https://doi.org/10.2514/1.6863

[37] Xiong, T., Yan, X., Huang, S., Yu, J., and Huang, Y., "Modeling and Analysis of Supercritical Flow Instability in Parallel Channels," *International Journal of Heat and Mass Transfer*, Vol. 57, No. 2, 2013, pp. 549–557.
https://doi.org/10.1016/j.ijheatmasstransfer.2012.08.046

[38] Liu, F., Lv, J., Zhang, B., and Yang, Z.," Nonlinear Stability Analysis of Ledinegg Instability Under Constant External Driving Force," *Chemical Engineering Science*, Vol. 206, Oct. 2019, pp. 432–445.
https://doi.org/10.1016/j.ces.2019.05.035

[39] Ruan, B., Huang, S., Meng, H., and Gao, X. W., "Transient Responses of Turbulent Heat Transfer of Cryogenic Methane at Supercritical Pressures," *International Journal of Heat and Mass Transfer*, Vol. 109, June 2017, pp. 326–335.
https://doi.org/10.1016/j.ijheatmasstransfer.2017.02.006

[40] Ambrosini, W., "Assessment of Flow Stability Boundaries in a Heated Channel with Different Fluids at Supercritical Pressure," *Annals of Nuclear Energy*, Vol. 38, Nos. 2–3, 2011, pp. 615–627.
https://doi.org/10.1016/j.anucene.2010.09.008

[41] Guo, Y., Bi, Q. C., Liu, Z. H., Yang, Z. Q., and Jiang, L., "Experimental Investigation on Thermal-Hydraulic Characteristics of Endothermic Hydrocarbon Fuel in 1 mm and 2 mm Diameter Mini-Channels," *Applied Thermal Engineering*, Vol. 122, July 2017, pp. 420–428.
https://doi.org/10.1016/j.applthermaleng.2017.05.038